molecules

MDPI

Article

Anti–Zika Virus Activity and Isolation of Flavonoids from Ethanol Extracts of *Curatella americana* L. Leaves

Lienne D'Auria Lima [1], Adriana Cotta Cardoso Reis [1], Jordano Augusto Carvalho Sousa [1], Gabriel Mendonça Valente [1], Breno de Mello Silva [2], Cíntia Lopes de Brito Magalhães [2], Markus Kohlhoff [3], Luiz Fernando de Medeiros Teixeira [4] and Geraldo Célio Brandão [1,*]

[1] Departamento de Farmácia, Escola de Farmácia, Universidade Federal de Ouro Preto, Campus Morro do Cruzeiro, Ouro Preto 35.400-000, MG, Brazil
[2] Departamento de Ciências Biológicas, Instituto de Ciências Exatas e Biológicas, Universidade Federal de Ouro Preto, Campus Morro do Cruzeiro, Ouro Preto 35.400-000, MG, Brazil
[3] Laboratório de Química de Produtos Naturais Bioativos, Fundação Oswaldo Cruz. Instituto René Rachou, Belo Horizonte 30.190-009, MG, Brazil
[4] Departamento de Análises Clínicas, Escola de Farmácia, Universidade Federal de Ouro Preto, Campus Morro do Cruzeiro, Ouro Preto 35.400-000, MG, Brazil
* Correspondence: celiobrandao@ufop.edu.br; Tel.: +55-31-3559-1088; Fax: +55-31-3559-1069

Abstract: The ethnomedicinal plant *Curatella americana* L. (Dilleniaceae) is a common shrub in the Brazilian Cerrado, whose ethanolic extract showed significant in vitro anti–Zika virus activity by the MTT colorimetric method. Currently, there is no drug in clinical use specifically for the treatment of this virus; therefore, in this work, the antiviral and cytotoxic properties of the ethanolic extract, fractions, and compounds were evaluated. The ethanolic extract of the leaves showed no cytotoxicity for the human MRC-5 cell and was moderately cytotoxic for the Vero cell (CC_{50} 161.5 ± 2.01 μg/mL). This extract inhibited the Zika virus multiplication cycle with an EC_{50} of 85.2 ± 1.65 μg/mL. This extract was fractionated using the liquid–liquid partition technique, and the ethyl acetate fraction showed significant activity against the Zika virus with an EC_{50} of 40.7 ± 2.33 μg/mL. From the ethyl acetate fraction, the flavonoids quercetin-3-*O*-hexosylgallate (**1**), quercetin-3-*O*-glucoside (**2**), and quercetin (**5**) were isolated, and in addition to these compounds, a mixture of quercetin-3-*O*-rhamnoside (**3**) and quercetin-3-*O*-arabinoside (**4**) was also obtained. The isolated compounds quercetin and quercetin-3-O-hexosylgallate inhibited the viral cytopathic effect at an EC_{50} of 18.6 ± 2.8 and 152.8 ± 2.0, respectively. Additionally, analyses by liquid chromatography coupled to a mass spectrometer allowed the identification of another 24 minor phenolic constituents present in the ethanolic extract and in the ethyl acetate fraction of this species.

Keywords: *Curatella americana*; Zika virus; cytotoxicity; phytochemistry; flavonoid

check for updates

Citation: Lima, L.D.; Reis, A.C.C.; Sousa, J.A.C.; Valente, G.M.; de Mello Silva, B.; Magalhães, C.L.d.B.; Kohlhoff, M.; Teixeira, L.F.d.M.; Brandão, G.C. Anti–Zika Virus Activity and Isolation of Flavonoids from Ethanol Extracts of *Curatella americana* L. Leaves. *Molecules* **2023**, *28*, 2546. https://doi.org/10.3390/molecules28062546

Academic Editor: Irinel Adriana Badea

Received: 5 February 2023
Revised: 23 February 2023
Accepted: 6 March 2023
Published: 10 March 2023

1. Introduction

Zika virus (ZIKV) is an arbovirus belonging to the family Flaviviridae, genus *Flavivirus*, and it is transmitted by mosquitoes of the genus *Aedes*. The virus was first isolated in 1947 in Uganda, Africa, and by 2007, very few human cases were described, all of which were associated with mild clinical symptoms [1]. However, since 2007, ZIKV has spread explosively and unexpectedly, infecting millions of people worldwide and in some cases even causing death [2,3].

ZIKV is believed to have led to a global crisis due to its unexpected links with testicular damage [4], eye damage [5], Guillain–Barré syndrome, fetal microcephaly [6,7], and potentially other neural complications. This emerging pathogen is an RNA virus, and although ZIKV is an arthropod-borne virus, transmission through sexual contact has also been reported [8].

Published results have shown that four different platforms are being used to develop ZIKV vaccines. While there are strong candidates for ZIKV vaccines, which protected rats and *Rhesus monkeys* from lethal ZIKV changes, their safety and cost issues still need to be addressed before becoming licensable vaccines that have a significant impact on overall health [9–11].

However, to date, there is no approved vaccine against Zika, and there is an imminent risk of the virus emerging and re-emerging in several countries around the world due to the prevalence of vectors and the high volumes of trade and travel [12], as well as considering the severe symptoms, such as Zika fever, microcephaly, birth defects, and Guillain–Barré syndrome [13].

Antiviral treatments against ZIKV are therefore necessary not only to end ZIKV-associated morbidities but also to disrupt the chain of transmission. Some broad-spectrum antivirals, such as interferons, ribavirin, and favipiravir, are not suitable for use against ZIKV as they may be harmful to pregnant women [14].

Despite continuous progress in the development of new antivirals, viral infections are still one of the leading causes of death worldwide. These infections can be controlled through either prophylactic or curative therapeutic measures. However, since viruses are metabolically inert particles, they need the metabolic pathways of living host cells to multiply, which makes it difficult to design efficient treatment modalities without causing damage to host cells [15,16]. Thus, considerable efforts have been made to find antiviral substances with satisfactory therapeutic effects and/or with new mechanisms of action, with higher plants presenting an excellent potential for prospecting for antiviral substances. The knowledge that plants have a variety of chemical constituents capable of inhibiting the cytopathic effect of viruses with different multiplication cycles makes it important to research natural products with this activity [16]. Our research group has shown that several species rich in phenolic compounds, such as flavonoids, are promising sources of substances with anti-ZIKV activity [17–21].

The phytochemical study of medicinal plants is a strategic alternative in the search for new therapeutic agents. The bibliographic survey and popular knowledge serve as the basis for identifying the pharmacological activity of medicinal plants. In the Brazilian Cerrado, there is great diversity of species and environments, making this biome have a high potential for use [22,23].

One of the highlights of the Cerrado due to its abundance is the species *Curatella americana*, popularly known as lixeira, cajueiro-bravo, or sambaíba, which is the only representative of the genus *Curatella* found in Brazil [24]. The species was identified by [25] as having a high value of ecological importance, when compared with other 63 species in the Cerrado strict sense area. It has a wide distribution with some penetration in the Amazon and Pantanal [26].

The beneficial effects of *C. americana* have been described in scientific research, and it is indicated by its popular use. The anti-inflammatory, analgesic, antihypertensive, hypolipidemic, antimicrobial, antioxidant, antileishmanial, antiulcerogenic, antifungal, and vasodilatory effects of the hydroethanolic extract of stems and leaves of *Curatella americana* L. were evaluated [24,27–32].

Despite being an important species of the Cerrado biome, there are relatively few chemical studies of extracts from this plant for medical use. El-Azizi et al. reported the isolation and identification of the flavonol glycoside avicularin and gallic acid [33]. Recent work using liquid chromatography techniques coupled to mass detectors identified a series of phenolic compounds, such as kaempferol, quercetin, and their glycosylated derivatives [34,35].

In this study, we carried out a survey of potential natural antiviral products belonging to plants native to the Cerrado biome and extracts from the leaves of *C. americana*, which showed very promising anti–Zika virus activity. Thus, this species was chosen for a bioguided phytochemical investigation due to its antiviral activity, resulting in the isolation

of five flavonols. Additionally, we performed analyses using liquid chromatography coupled to a mass spectrometer to identify some minor constituents.

2. Results and Discussion

Extracts obtained from *C. americana* have been studied in different biological models [28–32]. However, few works report the isolation of chemical constituents of this plant species. In this biography study, three flavonoids were isolated, including quercetin (**5**), quercetin-3-*O*-glucoside (**2**), and quercetin-3-*O*-hexosylgallate (**1**). Additionally, a mixture containing quercetin-3-*O*-rhamnoside (**3**) and quercetin-3-*O*-arabinoside (**4**) was also obtained. The structures of the isolated compounds are shown in Figure 1 All isolated compounds were subjected to analysis by ^{1}D and ^{2}D NMR spectra shown in the Supplementary Material Section (Figures S1–S29). In these spectra, it is possible to observe that the carbons located in position 3 of the flavonic genin have a chemical shift (δ) between 135.0 and 137.0 ppm. This is characteristic of oxygenated flavonoids at this position. Signs of hydrogenated carbons with chemical shifts compatible with positions 6 and 8 of genin (δ 94.0 and 100.0 ppm, respectively) are also observed. Additionally, signals are observed in more shielded regions of the spectra, attributed to sugar residues. All ^{13}C and ^{1}H NMR data are described in the Materials and Methods section. The data obtained from the NMR analyses suggest that it is a series of oxygenated flavonoids at carbon 3. The structure confirmation of the isolated compounds was obtained by analyzing the UPLC–DAD–HRMS data, and with these data, it was possible to obtain the molar mass of each compound and also the UV data with bands I and II; thus, that exhibits maximum absorption characteristic of flavonoids (Table 1).

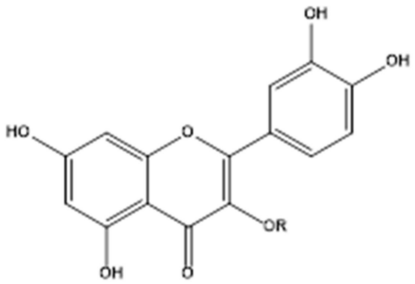

(1) R = glucose–gallic acid

(2) R = glucose

(3) R = rhamnose

(4) R = arabinose

(5) R = H

Figure 1. Chemical structures of flavonoids from the leaves of *Curatella americana*.

Table 1. Spectroscopic data and characterization of polyphenols in leaf ethanolic extract from *Curatella americana* by UPLC–ESI–MS/MS.

	Compounds	Molecular Formula	RT * (min)	UV (nm)	[M-H]$^{-}$ (*m*/*z*)	Characteristic *m*/*z* of Ions in Positive Ion Mode (%)	HRMS [M + H]$^{+}$ (*m*/*z*)	Error (ppm)
1	(Epi)catechin	$C_{15}H_{14}O_6$	13.1	278	288.95	291.0860 (30.02), 139.0387 (100.0), 123.0437 (45.4)	291.0858	3.4
2	(Epi)catechin	$C_{15}H_{14}O_6$	14.3	279	289.14	291.0859 (34.8), 147.0439 (24.3), 139.0386 (100.0)	291.0859	3.1
3	B-type dimer of (epi)catechin-(epi)catechin-*O*-gallate	$C_{37}H_{30}O_{16}$	14.4	277	729.27	731.1636 (16.4), 579.1163 (13.4), 291.0860 (12.8), 153.0180 (100.0)	731.1607	0.7
4	Homoorientin	$C_{21}H_{20}O_{11}$	15.3	265, 350	447.17	449.1087 (73.1), 329.0650 (71.7), 299.0546 (100.0)	449.1074	2.0

Table 1. *Cont.*

	Compounds	Molecular Formula	RT * (min)	UV (nm)	[M-H]$^-$ (*m*/*z*)	Characteristic *m*/*z* of Ions in Positive Ion Mode (%)	HRMS [M + H]$^+$ (*m*/*z*)	Error (ppm)
5	Orientin	$C_{21}H_{20}O_{11}$	15.5	265, 350	447.26	449.1084 (100.0), 329.0651 (67.0), 299.0546 (38.7)	449.1077	1.3
7	Quercetin-3-*O*-hexosyl-arabinoside	$C_{26}H_{28}O_{16}$	15.5	269, 350	595.33	597.1469 (1.8), 465.1037 (7.7), 303.0500 (100.0)	597.1449	1.8
8	Quercetin-3-*O*-hexosylgallate	$C_{28}H_{24}O_{16}$	16.0	264, 354	615.20	617.1156 (18.8), 303.0500 (97.3), 153.0182 (100.0)	617.1137	1.0
9	Isovitexin	$C_{21}H_{20}O_{10}$	16.1	267, 350	431.09	433.1138 (100.0), 313.0708 (59.2), 283.0600 (42.9)	433.1129	1.1
10	Vitexin	$C_{21}H_{20}O_{10}$	16.2	267, 351	431.23	433.1137 (100.0), 313.0709 (57.3), 283.0601 (42.2)	433.1130	0.9
11	Quercetin-3-*O*-glucoside	$C_{21}H_{20}O_{12}$	16.3	256, 354	463.17	465.1035 (2.0), 303.0501 (100.0)	465.1030	0.6
12	Kaempferol-3-*O*-hexosyl-arabinoside	$C_{26}H_{28}O_{15}$	16.4	256, 354	579.20	449.1083 (11.1), 287.0552 (100.0)	581.1499	1.2
13	Kaempferol-3-*O*-hexosylgallate	$C_{28}H_{24}O_{15}$	16.5	269,353	599.06	601.1212 (7.4), 287.0549 (100.0), 153.0181 (75.5)	601.1185	1.3
14	Quercetin-3-*O*-arabinoside	$C_{20}H_{18}O_{11}$	16.8	256, 354	433.32	435.0927 (1.2), 303.0500 (100.0), 153.0182 (2.7)	435.0922	1.1
15	Methylquercetin-3-*O*-glucuronylgallate	$C_{29}H_{26}O_{16}$	16.8	270, 365	629.24	631.1308 (9.5), 329.0868 (19.1), 303.0500 (59.7), 167.0341 (100.0)	631.1291	1.3
16	Kaempferol-3-*O*-hexosylgallate	$C_{28}H_{24}O_{15}$	17.1	257, 354	599.25	601.1209 (19.7), 315.0711 (18.8), 287.0551 (99.3), 153.0183 (100.0)	601.1189	0.7
17	Kaempferol-3-*O*-glucoside	$C_{21}H_{20}O_{11}$	17.4	256, 349	447.30	287.0551 (100.0), 153.0182 (4.4)	449.1079	0.9
18	Quercetin-3-*O*-rhamnoside	$C_{21}H_{20}O_{11}$	17.5	256, 348	447.17	303.0503 (100.0), 153.0182 (11.7)	449.1080	0.7
19	Quercetin-3-*O*-hexosyl-*O*-acetyl	$C_{23}H_{22}O_{13}$	17.6	256, 354	505.18	507.1143 (8.4), 303.0501 (100.0), 187.0599 (6.3)	507.1133	1.0
20	Kaempferol-3-*O*-arabinoside	$C_{20}H_{18}O_{10}$	17.7	256, 354	417.31	419.0967 (2.1), 287.0551 (100.0), 153.0184 (3.7)	419.0973	1.2
21	Quercetin-3-*O*-hexosyl-*O*-acetyl	$C_{23}H_{22}O_{13}$	18.0	256, 354	505.21	507.1145 (3.6), 303.0501 (100.0), 205.0707 (3.3)	507.1135	0.6
22	Kaempferol-3-*O*-rhamnoside	$C_{21}H_{20}O_{10}$	18.5	270, 355	431.29	287.0552 (100.0), 153.0182 (2.6)	433.1130	0.9
23	Quercetin-3-*O*-arabinosyl-O-acetyl	$C_{22}H_{20}O_{12}$	18.7	256, 354	475.13	303.0501 (100.0), 175.0602 (12.2)	477.1028	1.0
24	Kaempferol-3-*O*-hexosyl-*O*-acetyl	$C_{23}H_{22}O_{12}$	18.8	256, 354	489.17	287.0550 (100.0), 187.0603 (5.9)	491.1184	1.0

Table 1. *Cont.*

	Compounds	Molecular Formula	RT * (min)	UV (nm)	[M-H]$^-$ (*m*/*z*)	Characteristic *m*/*z* of Ions in Positive Ion Mode (%)	HRMS [M + H]$^+$ (*m*/*z*)	Error (ppm)
25	Quercetin-3-*O*-(6″-*O*-*E*-*p*-coumaroyl)-glucopyranoside	$C_{30}H_{26}O_{14}$	19.2	277, 354	609.25	611.1407 (4.9), 303.0500 (25.8), 147.0441 (100.0)	611.1394	2.3
26	Quercetin	$C_{15}H_{10}O_7$	20.1	275, 371	301.29	303.0500 (100.0), 229.0496 (7.4), 153.0182 (10.5), 137.0232 (4.5)	303.0498	2.0
27	Kaempferol-3-O-(6″-*O*-*E*-*p*-coumaroyl)-glucopyranoside	$C_{30}H_{26}O_{13}$	20.2	277, 350	593.18	595.1456 (4.2), 309.0968 (15.3), 287.0549 (29.4), 147.0441 (100.0)	595.1446	0.8
28	Kaempferol-3-O-(2″-*O*-*E*-*p*-coumaroyl)-glucopyranoside	$C_{30}H_{26}O_{13}$	20.6	254, 369	593.31	595.1459 (7.6), 309.0965 (7.3) 287.0549 (65.4), 147.0440 (100.0)	595.1444	1.2
29	Kaempferol	$C_{15}H_{10}O_6$	22.0	269, 350	285.09	287.0550 (100.0), 153.0180 (14.5), 137.0232 (2.2)	287.0548	2.4

* Retention time obtained in chromatographic/HRMS analysis.

Figure 2 shows the chromatographic profiles of the leaf extract and the fractions obtained in the liquid–liquid partition. The qualitative analysis of these chromatographic profiles suggests that the process employed was efficient in concentrating the flavonoids in the ethyl acetate fraction.

The results are in agreement with the literature reported for the chemistry of this plant species from which quercetin-3-*O*-arabinoside and gallic acid have already been isolated [33]. Recent work analyzing leaf extracts of the species by UPLC–MS also identified flavonoids as major constituents [34,35].

In order to identify minor phenolic constituents from the ethanolic extract and ethyl acetate fraction active in antiviral assays, analyses using UPLC–MS and MS/MS were performed. The data obtained in these analyses are compiled in Table 1. After a careful analysis of the data, it was possible to identify 24 phenolic compounds in addition to the compounds already isolated. These results once again demonstrate that extracts from this plant species are promising sources for obtaining flavonoids.

The cytotoxicity of ethanolic extracts of stems, leaves, fractions, and substances isolated from the *C. americana* species was evaluated by the colorimetric MTT method in Vero cell lines (derived from African green monkey kidneys) and MRC-5 (derived from normal human lung tissue). The results of CC_{50} are described in Table 2.

According to the literature, crude extracts whose $CC_{50} \leq 20$ µg/mL are classified as extracts with high cytotoxic effect [36], and those extracts with $CC_{50} > 100.0$ µg/mL are not considered cytotoxic [37]. Thus, for the ethanolic extract of C. americana stems, moderate cytotoxicity was observed for Vero cells ($CC_{50} = 54.4$ µg/mL) and no cytotoxicity was observed for MRC-5 cells ($CC_{50} > 400.0$ µg/mL). Meanwhile, the leaf extract was considered noncytotoxic for both cell lines: Vero ($CC_{50} = 161.5$ µg/mL) and MRC-5 ($CC_{50} > 400.0$ µg/mL).

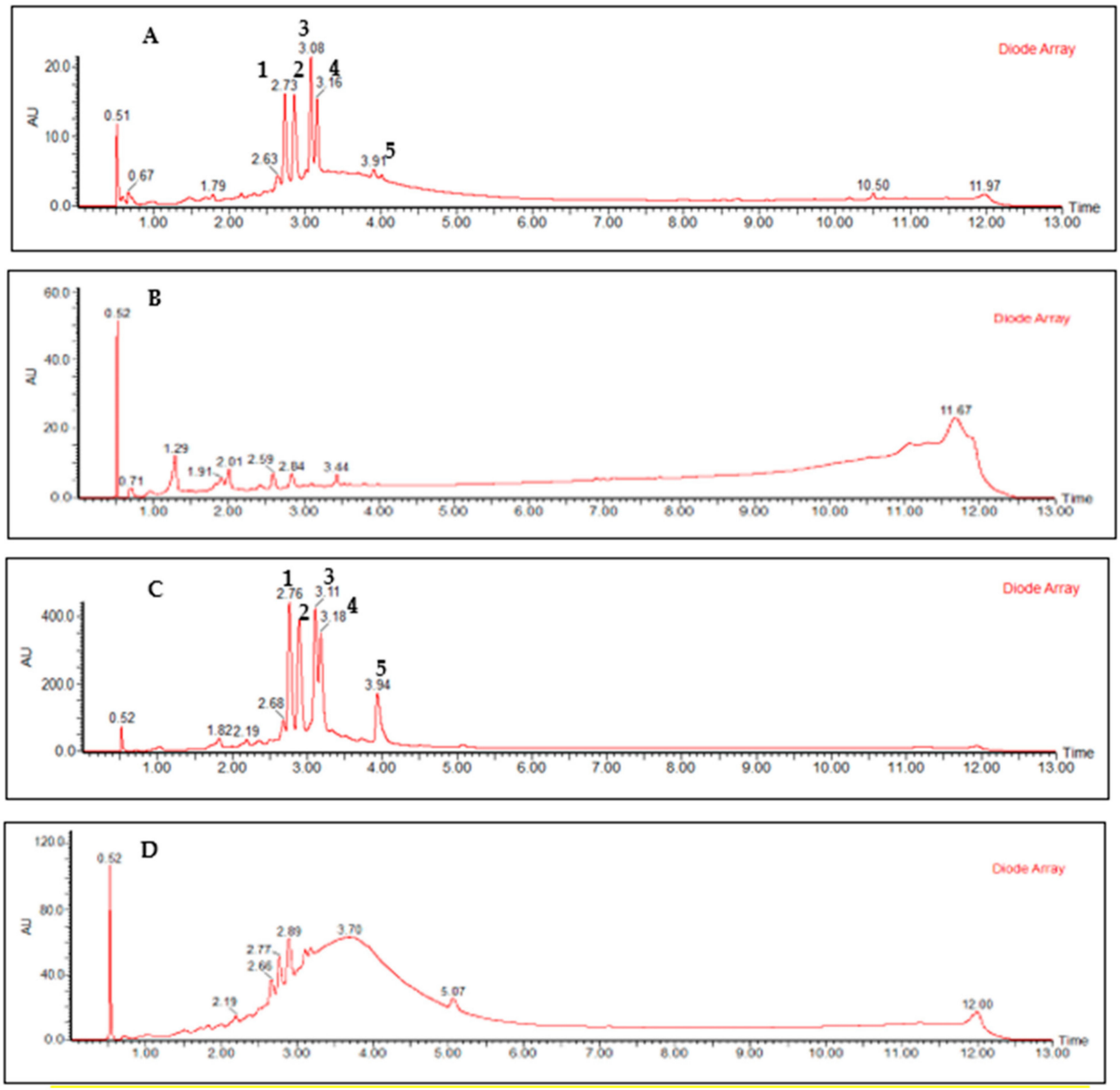

Figure 2. RP-UPLC-DAD profile of ethanolic extract (**A**), dichloromethane fraction (**B**), ethyl acetate fraction (**C**), and aqueous fraction (**D**) of *Curatella americana* leaves. Conditions: CHS130 100 RP-18 column (1.7 µm, 50 × 3 mm i.d.). Elution was carried out with a linear gradient of water with 0.1% formic acid and acetonitrile with 0.1% formic acid (from 5% to 95% of acetonitrile with 0.1% formic acid in 11 min), and the UPLC fingerprints were registered on an Acquity (Waters, Milford, Massachusetts, USA) apparatus with a UV-DAD detector (Waters 2996). (**1**) Quercetin-3-*O*-hexosylgallate, (**2**) quercetin-3-*O*-glucoside, (**3**) quercetin-3-*O*-rhamnoside, (**4**) quercetin-3-*O*-arabinoside, and (**5**) quercetin.

Table 2. Anti–Zika virus activity and its standard deviations (n = 3) of ethanolic extracts of stems and leaves, fractions, substances isolated from *Curatella americana*.

Extracts	Used Part	CC_{50} Vero µg/mL	CC_{50} MRC-5 µg/mL	EC_{50} µg/mL	SI Vero	SI MRC-5
Curatella americana	Stems	54.6 ± 1.4	>400	Inactive	-	-
Curatella americana	Leaves	161.5 ± 2.0	>400	85.2 ± 1.6	1.9	>2.5
Fractions						
Fraction DCM	Leaves	58.9 ± 1.3	115.2 ± 1.8	Inactive	-	-
Fraction AcOEt	Leaves	56.2 ± 1.2	>400	40.7 ± 2.3	1.4	9.8
Fraction H_2O/MeOH	Leaves	101.0 ± 1.2	>400	Inactive	-	-
Isolated Compounds						
Quercetin-3-*O*-hexosylgallate	Leaves	305.6 ± 1.4 (496.1 ± 1.4 µM)	>100 (>162.3 µM)	152.8 ± 2.0 (248.1 ± 2.0 µM)	2.0	>0.7
Quercetin-3-*O*-glucoside	Leaves	>100 (>215.5 µM)	>100 (>215.5 µM)	Inactive	-	-
Quercetin	Leaves	71.3 ± 1.3 (235.8 ±1.3 µM)	NT	18.61 ± 2.8 (61.6 ± 2.8 µM)	3.8	-
Ribavirin (positive control)	-	370.4 ± 1.2 (1516.7 ± 1.2 µM)	NT	94.47 ± 2.7 (386.8 ± 2.7 µM)	3.9	-

These cell lines are two nontumor transformed cell lines, and they have distinct characteristics. The Vero cell was deleted by -9-Mb on chromosome 12, which contained the CDKN2A and CDKN2B genes. CDKN2A encodes two cyclin-dependent kinase inhibitors, p16INK4A (which inhibits CDK6, a negative regulator of pRB retinoblastoma protein) and p14 ARF (which inhibits p53-negative regulator MDM2); CDKN2B already encodes the p15INK4B inhibitor (which inhibits another pKR CDK4 negative regulator). Loss of both genes plays a crucial role in the acquisition of immortality in the Vero cell line [38–40]. For MRC-5 cells, their immortality is related to the ectopic expression of the telomerase catalytic subunit (hTERT); the expression of this gene allows normal human cells to bypass senescence and, consequently, become immortal [41,42]. These differences may be related to the observed toxicity profile, which may indicate selective cytotoxic activity, an important parameter when searching for a substance with antineoplastic activity.

The evaluation of cytotoxicity in Vero cells is essential to be carried out prior to the antiviral activity assays to determine the concentration of extracts, in which cell viability corresponds to 50% (CC_{50}), so that the antiviral assay can be performed from lower concentrations to CC_{50} [43].

MRC-5 cells are widely used in the assessment of cytotoxicity in parallel with biological activity screening assays due to their sensitivity and receptivity to various microorganisms [37]. Thus, the cytotoxicity in MRC-5 cells was performed with the purpose of inferring from this normal human cell line the cytotoxic potential of the extracts in human cells, and the low cytotoxicity in human cells is considered a favorable factor to proceed with the research of the antiviral activity of these extracts.

The results found in Vero cells for ethanolic extracts of *C. americana* stems and leaves in the present study are in line with literature data. De Toledo et al. [30] performed a Vero cell cytotoxicity test for the ethanolic extract of *C. americana* stems, and the result was very similar to that described in this study, with a CC_{50} of 53.3 µg/mL. In this work, the authors suggest that a moderate cytotoxic activity of this species is related to saponins and tannins present in the extracts [30]. According to Costa et al. [28], saponins interact strongly with the cell membrane, while tannins interact strongly with proteins, and these interactions are directly related to their chemical structures.

In the fractions obtained from the partition of the ethanolic extract of *C. americana* leaves, we can observe that the cytotoxicity results in Vero cells compared with MRC-5 cells are very different from each other. The EtOAc and DCM fractions showed moder-

ately cytotoxic results for Vero cells with a CC_{50} of 56.2 and 58.9 µg/mL, respectively, while H_2O/MeOH presented a CC_{50} of 101.0 µg/mL, which is considered noncytotoxic. For MRC-5 cells, no cytotoxicity was observed to the EtOAc and H_2O/MeOH fractions (CC_{50} > 400.0 µg/mL) and to the DCM fraction (CC_{50} = 115.2 µ/mL). Despite that, according to Cos et al., the leaf extract fractions are not considered cytotoxic [37].

This cytotoxic difference can be explained by the fact that the transformations/mutations that occurred for each cell type with the goal of immortality are distinct from each other, directly impacting the selectivity of cytotoxicity, as occurs in stem and leaf extracts of this species [38,41]. Moreover, it is noteworthy that they are cell lines belonging to different animal species, which perform different functions in the organisms in which they live.

As for the isolated substances, quercetin-3-*O*-glucoside was not cytotoxic in the highest concentration tested (100.0 µg/mL) for both cell lines. Quercetin showed a CC_{50} of 235.8 µM (71.3 µg/mL) in Vero cell, and quercetin-3-*O*-hexosylgallate presented a CC_{50} of 496.1 µM (305.6 µg/mL) in Vero cell; also, it was noncytotoxic in the highest concentration tested (100.0 µg/mL).

These results of low or noncytotoxic activity are a favorable prognosis for testing biological activities, including antiviral, considering that when given a positive result, it can be said that the compound shows selectivity for infected cells.

After the determination of optimal noncytotoxic use concentrations, assays were performed, treating ZIKV-infected Vero cells with eight concentrations from the noncytotoxic concentrations for each sample. The results of the 50% effective concentration (EC_{50}—concentration of the substance capable of reducing the viral cytopathic effect by 50%) and selectivity index (SI) are described in Table 2.

According to the chromatographic profile of *C. americana* leaf extract, we can observe that flavonoids-*O*-glycosylated were identified for this species. In general, flavonoids exhibit a multitude of biological activities, including antiviral activity against influenza viruses [44], hepatitis C [45], cytomegalovirus [46], dengue [47], Zika [48], and chikungunya [49]. Literature data show that flavonol-*O*-glycosylated, more specifically quercetin-3-*O*-glucoside, exhibits potent anti–Zika virus activity in Vero cell lines, A549 (human pulmonary epithelial cell), Huh-7 (human hepatoma cell), and SH-SY5Y (human neuroblastoma cell) [48,50]. In addition, it has recently been reported that epigallocatechin gallate (EGCG) and curcumin are also effective against ZIKV [49,51]. Thus, the phytochemical investigation sought the isolation of these flavonoids in the extract of leaves of *C. americana*, because they are believed to be responsible for the antiviral activity observed in the extract (Table 2 and Figure 3).

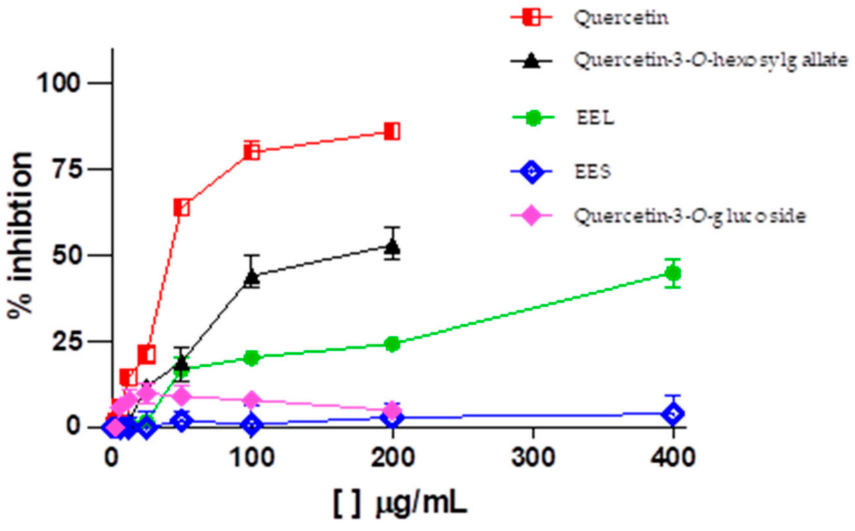

Figure 3. Dose–response curves for anti-Zika activity of ethanolic extracts and constituents from *Curatella americana* (EEL—ethanol extract of leaves, EES—ethanol extract of stems).

Corroborating with expectations, the ethyl acetate fraction, flavonoid rich, was the only fraction that showed significant anti–Zika virus activity with an EC_{50} of 40.7 μg/mL. There were three isolated substances obtained, where quercetin-3-*O*-hexosylgallate and quercetin registered activity against the Zika virus with an EC_{50} of 248.1 μM (152.8 μg/mL) and 61.6 μM (18.6 μg/mL), respectively, and quercetin-3-*O*-glucoside was not active (Figure 3).

Contrary to literature results, quercetin-3-*O*-glucoside isolated in this study did not show activity against Zika virus at the highest concentration tested (100.0 μg/mL) in the Vero cell line. This can be explained by the low quercetin-3-*O*-glucoside concentration used in the tests and increased viral titer compared with the study by Wong et at. [48], which used a concentration of 400.0 μg/mL quercetin-3-*O*-glucoside and an infection multiplicity of 0.05.

The activity of quercetin-3-*O*-hexosylgallate is believed to be related to the presence of the gallate group, given that this group was responsible for the anti–Zika virus activity determined for the flavonoid EGCG according to Sharma et al. [51].

Quercetin is a flavonol known for several properties, such as its antioxidant, antimicrobial, anticancer, antiviral, and anti-inflammatory effects. Recent studies have highlighted the potential use of quercetin as an antiviral, justified by its ability to inhibit the initial stages of virus infection, interact with proteases important for viral replication, and reduce inflammation caused by viral infection [52].

Our results corroborate with the literature, as demonstrated by Roy et al. [53] and Lim et al. [54], that quercetin is able to inhibit the ZIKV protease NS2B–NS3pro, which is absolutely essential for cleaving the ZIKV polyprotein into functional subunits. Additionally, the structure–activity relationship study performed by Zou et al. [55] demonstrated quercetin inhibiting the ZIKV infection by disrupting the virus entry and also by targeting the viral protease NS2B–NS3.

The results obtained in the in vitro cytopathic effect inhibition assay demonstrated that the cell monolayer infected by Zika virus allows viral multiplication inside the cells, leading to the cell monolayer destruction that was observed in the image (Figure 4B). This can be seen by the destruction and morphological alterations of the cells, such as rounding of cells, formation of lumps, and changes in cell refringence, especially when compared with the uninfected and untreated cell monolayer (Figure 4A).

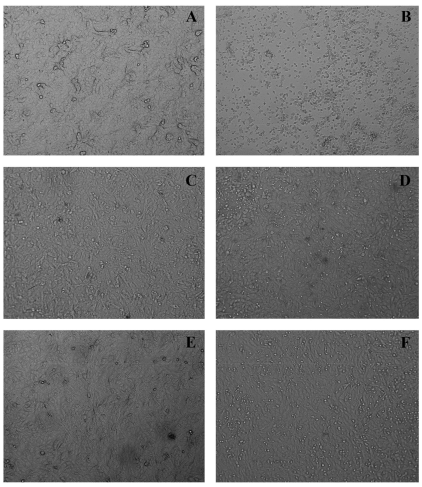

Figure 4. Antiviral effect against Zika virus in Vero cells treated with ethanol extract of leaves and quercetin. Vero cells were infected with ZIKV, treated with ethanol extract of leaves/quercetin, and photographed after 48 h of infection. (**A)** Uninfected and untreated cells, (**B**) infected cells, (**C**) cells uninfected and treated with ethanol extract of leaves (85 μg/mL), (**D**) cells infected and treated with ethanol extract of leaves (85 μg/mL), (**E**) cells uninfected and treated with quercetin (20 μg/mL), (**F**) cells infected and treated with quercetin (20 μg/mL). Magnification, 100x.

While treating the ZIKV-infected cell monolayer with extracts and/or isolated quercetin, it is possible to protect the cells from a virus infection and thus prevent cell death once the cells remain attached (such as a monolayer) and no morphocellular deformities are observed. Therefore, they indicate that the treatment performed after infection is effective in inhibiting the virus multiplication cycle, confirming the antiviral activity observed in the MTT colorimetric assay.

This suggests that quercetin-like flavonoids are interesting drugs with selective and relevant in vitro anti–Zika virus activity. Therefore, future studies of these compounds may provide relevant data for the production of antivirus molecules.

3. Materials and Methods

3.1. General Experimental Procedures

The isolated compounds were submitted to ^{1}D and ^{2}D ^{1}H and ^{13}C-NMR spectra, such as COSY, HSQC, and HMBC, which were obtained on a Bruker Avance DRX 400 instrument (Bruker®, Billerica, MA, USA). Tetramethylsilane (TMS) was used as an internal reference, and deuterated methanol (CD_3OD, Cambridge Isotope Laboratories, Inc.,® Tewksbury, MA, USA) was used as a solvent.

In the TLC analyses on silica gel 60 (Merck®, Kenilworth, NJ, USA), ethyl acetate/formic acid/acetic acid/water (100:11:11:27) was used as mobile phase NP/PEG developer (Sigma-Aldrich®, San Luis, MO, USA) and as reference compounds quercetin (Sigma-Aldrich®, San Luis, MO, USA) and isoquercitrin (Sigma-Aldrich®, San Luis, MO, USA).

In preparing the samples for analysis by LC–MS, 2.5 mg of each extract and/or fractions were weighed directly into Eppendorf-type flasks, and 1.0 mL of ultrapure methanol (Merck®, Kenilworth, NJ, USA) was added. For the complete dissolution of the samples, sonication was used in an ultrasound bath; then the samples were centrifuged at 10,000 rpm for 5 min. The supernatant was filtered through 0.22 μm pore PVDF (polyvinylidene fluoride) filters and transferred to vials for use in CLUE-FR analysis.

3.2. Plant Material

The different parts of the plant (stems and leaves) of *Curatella americana* L. were collected in Santana de Pirapama (19°00′21′′ S and 44°02′34′′ W), Minas Gerais, Brazil. The taxonomic determinations were made by Prof. Maria Cristina Teixeira Braga Messias from the Department of Biodiversity, Evolution, and Environment in the Institute of Exact and Biological Sciences at the Federal University of Ouro Preto. The exsiccate was deposited at the Professor José Badini Herbarium (registration OUPR-UFOP 28723).

3.3. Preparation of Crude Extract and Fractionation

The different parts of the plants (leaves (1.2 kg) and stems (79.6 g)) were separated and dried in a ventilated oven at 40 °C. After drying, grinding was performed using a knife mill. The powders obtained were placed in amber glass bottles, each bottle being identified according to the part of the plant. The plant materials were subjected to exhaustive extraction by cold percolation with ethanol, obtaining extracts of stems (9.3 g) and leaves (490.0 g). The ethanolic extracts obtained were concentrated in a rotary evaporator (Buchi®, New Castle, DE, USA) under reduced pressure at a temperature of 45 °C. For complete removal of the solvent, the extract residues were transferred to previously weighed flasks and then carefully dried in an oven at 50 °C. The dry ethanolic extracts were submitted to cytotoxic and antiviral activity assays. Only the leaf extract inhibited the viral multiplication cycle, which was selected for the bioguided study.

In the preliminary fractionation of the leaf extract, the liquid–liquid partition technique with immiscible solvents was used. A portion of the extract (100.0 g) was solubilized in a methanol/water mixture (60:40) and sequentially partitioned with the organic solvents dichloromethane (DCM) and ethyl acetate (EtOAc) (3 times 100.0 mL each solvent). Thus, the DCM, EtOAc, and hydromethanolic (H_2O/MeOH) fractions were obtained (Figure 5). These organic solutions were concentrated by distillation under reduced pres-

sure on a rotary evaporator. The concentrated fractions obtained were transferred to previously weighed glass vials, dried in a 50 °C controlled temperature oven, and subsequently weighed.

3.4. Isolation and Identification of Flavonoids

Four portions of the ethyl acetate fraction (200.0 mg each) that was active in the antiviral assays were fractionated by size exclusion chromatography using Sephadex LH-20 resin (Pharmacia Biotech®, Raleigh, NC, USA) (Sephadex LH-20, 30.0 g, ø 70.0 µm; eluted with MeOH). In the fractionation of each portion, 40 fractions of 10.0 mL on average were collected. The fractions were subjected to analysis by thin-layer chromatography (TLC), and those with similar profiles were pooled. From the pooled fraction number 12, a yellow solid identified as quercetin-3-*O*-hexosylgallate (**1**) (7.0 mg) was obtained (Figure 5).

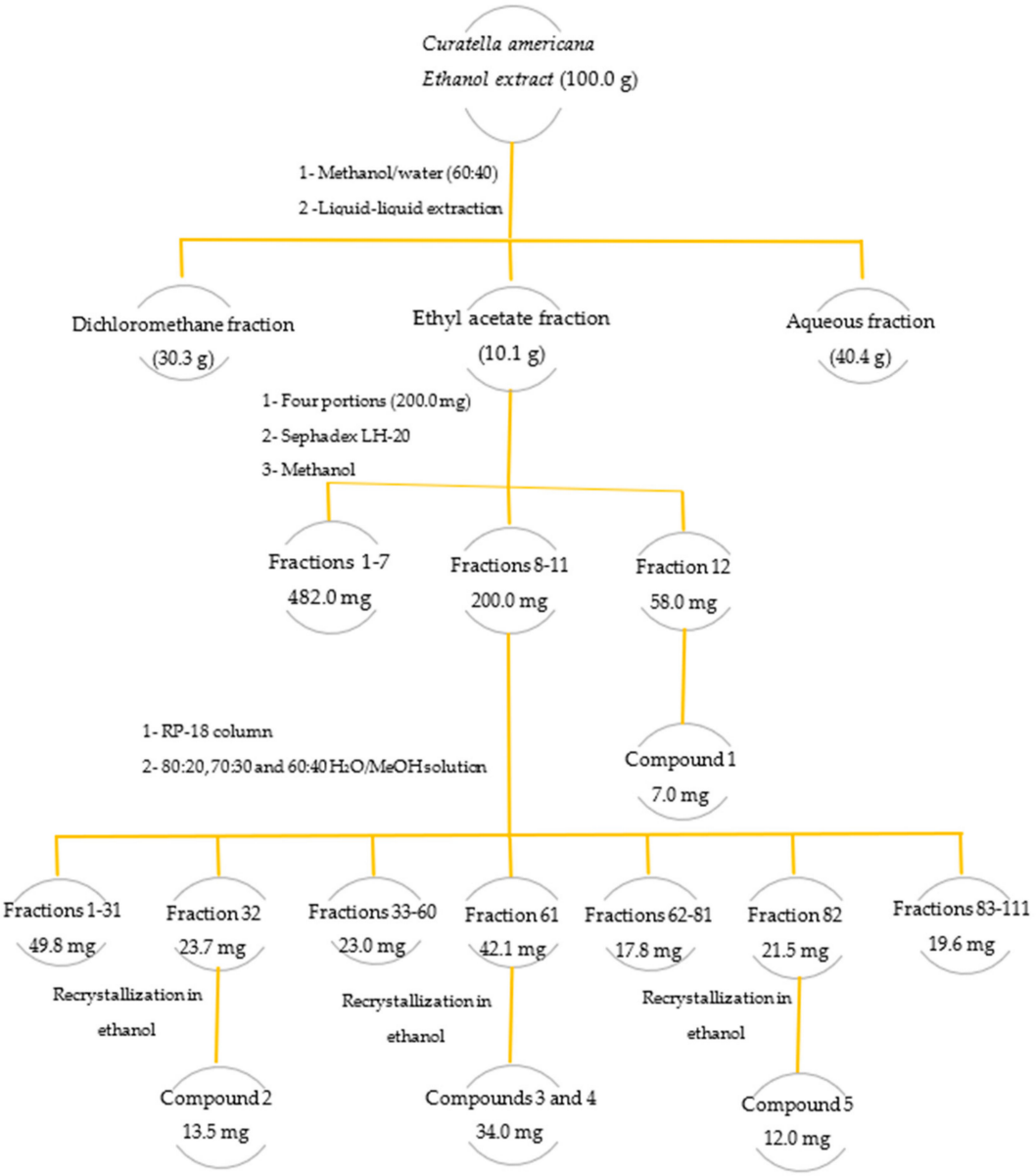

Figure 5. Fractionation of the ethanolic extract of leaves of the species *Curatella americana*.

Fractions 8 to 11 with a similar profile on TLC were pooled (totaling 200.0 mg) and subjected to fractionation by chromatography on a reversed-phase silica gel octadecylsilane column (Merck®, Kenilworth, NJ, USA, RP-18 column, 4 g, ø 10 µm; eluted with an 80:20,

70:30 and 60:40 H_2O/MeOH solution). A total of 220 fractions of approximately 5.0 mL were collected, grouped into 111 fractions after analysis by TLC. Fraction 32 resulted in the isolation of a yellow solid, called quercetin-3-*O*-glucoside (**2**), known as isoquercitrin (13.5 mg). In pooled fraction 61, a 34.0 mg mixture of the flavonoids quercetin-3-*O*-rhamnoside (**3**) and quercetin-3-*O*-arabinoside (**4**) were obtained. Fraction 82 was recrystallized with absolute ethanol from which 12.0 mg of a yellow solid identified as quercetin (**5**) was obtained (Figure 5).

The isolated compounds were identified by nuclear magnetic resonance (^{1}H NMR and ^{13}C NMR). The data were confirmed by two-dimensional techniques (DEPT, COSY, HSQC, HMBC) and by mass spectrometry. Additionally, the data obtained in this study were compared with data from the literature [56–59].

3.5. Spectroscopic Data for Isolated Compounds

Quercetin-3-*O*-hexosylgallate (compound 1): Yellowish powder, UV λ_{max} 264, 354 nm; ESI-MS *m*/*z*: $[M-H]^+$ 617.22, HRMS $[M+H]^+$ 617.1137, cald. for $C_{28}H_{25}O_{16}$ 617.1142 Da; ^{1}H-NMR (CD_3OD, 400 MHz, ppm) 6.18 (1H, d, *J* = 2.24 Hz, H-6), 6.37 (1H, d, *J* = 1.96 Hz, H-8), 7.78 (1H, d, *J* = 2.12 Hz, H-2′), 6.81 (1H, d, *J* = 8.48 Hz, H-5′), 7.55 (1H, m, H-6′), 5.11 (1H, d, *J* = 7.8 Hz, H-1′′), 3.85 (1H, m, H-2′′), 3.80 (1H, m, H-3′′), 3.87 (1H, m, H-4′′), 3.59 (1H, m, H-5′′), 4.09 (2H, q, H-6′′), 6.88 (2H, s, H-2′′′, H-6′′′); ^{13}C-NMR (CD_3OD, 400 MHz, ppm) 158.3 (C-2), 135.7 (C-3), 179.5 (C-4), 166.0 (C-5), 99.9 (C-6), 168.0 (C-7), 94.8 (C-8), 162.8 (C-9), 105.4 (C-10), 123.6 (C-1′), 117.7 (C-2′), 145.8 (C-3′), 149.9 (C-4′), 116.1 (C-5′), 123.0 (C-6′), 105.5 (C-1′′), 73.0 (C-2′′), 74.5 (C-3′′), 70.0 (C-4′′), 74.9 (C-5′′), 61.6 (C-6′′), 121.0 (C-1′′′), 109.8 (C-2′′′, 6′′′), 146.3 (C-3′′′), 145.8 (C-5′′′), 135.7 (C-4′′′), 173.1 (C-7′′′).

Quercetin-3-*O*-glucoside (compound 2): Yellowish powder, UV λ_{max} 255, 354 nm; ESI-MS m/z: $[M+H]^+$ 465.13, HRMS $[M+H]^+$ 465.1030, cald. for $C_{21}H_{21}O_{12}$ 465.1033; 1H NMR (400 MHz, CD_3OD, ppm) 6.26 (1H, d, *J* = 2,16 Hz, H-6), 6.08 (1H, d, *J* = 2.08 Hz, H-8), 7.59 (1H, d, *J* = 2.16 Hz, H-2′), 6.74 (1H, d, *J* = 8.48 Hz, H-5′), 7.46 (1H, dd, *J* = 8.48, 2.16 Hz, H-6′), 5.14 (1H, d, *J* = 7.4 Hz, H-1′′), 3.36 (1H, m, H-2′′), 3.34 (1H, m, H-3′′), 3.31 (1H, m, H-4′′), 3.11 (1H, m, H-5′′), 3.58 (1H, dd, *J* = 11.92, 2.16 Hz, Ha-6′′), 3.61 (1H, dd, *J* = 11.88, 5.2 Hz, Hb-6′′); ^{13}C NMR (400 MHz, CD_3OD, ppm) 158.6 (C-2), 135.7 (C-3), 179.6 (C-4), 163.1 (C-5), 100.0 (C-6), 166.1 (C-7), 94.8 (C-8), 159.1 (C-9), 105.8 (C-10), 123.3 (C1′), 117.7 (C-2′), 146.0 (C-3′), 149.9 (C-4′), 116.1 (C-5′), 123.2 (C-6′), 104.4 (C-1′′), 75.8 (C-2′′), 78.2 (C-3′′), 71.3 (C-4′′), 78.5 (C-5′′), 62.6 (C-6′′).

Quercetin-3-*O*-rhamnoside (compound 3): Yellowish powder, UV λ_{max} 256 and 349 nm; ESI–MS m/z: $[M+H]^+$ 449.13, HRMS $[M+H]^+$ 449.1080, cald. for $C_{21}H_{21}O_{11}$ 449.1083 Da; ^{1}H NMR (400 MHz, CD_3OD, ppm) 6.09 (1H, m, H-6), 6.27 (1H, m, H-8), 6.82 (1H, m, H-2′), 7.24 (1H, m, H-5′), 7.22 (1H, m, H-6′), 5.25 (1H, m, H-1′′), 3.80 (1H, m, H-2′′), 4.12 (1H, m, H-3′′), 3.32 (1H, m, H-4′′), 3.66 (1H, m, H-5′′), 0.83 (1H, m, H-6′′); ^{13}C NMR (100 MHz, CD_3OD, ppm), 159.4 (C-2), 136.4 (C-3), 179.6 (C-4), 163.2 (C-5), 100.0 (C-6), 166.2 (C-7), 94.8 (C-8), 158.5 (C-9), 105.7 (C-10), 123.1 (C1′), 116.5 (C-2′), 146.6 (C-3′), 149.9 (C-4′), 117.0 (C-5′), 123.0 (C-6′), 103.7 (C-1′′), 73.0 (C-2′′), 72.0 (C-3′′), 72.2 (C-4′′), 72.1 (C-5′′), 17.8 (C-6′′).

Quercetin-3-*O*-arabinoside (compound 4): Yellowish powder, UV λ_{max} 256 and 354 nm; ESI–MS m/z: [M+H]+ 435.15, HRMS $[M+H]^+$ 435.0922, cald. for $C_{20}H_{19}O_{11}$ 435.0927 Da; ^{1}H NMR (400 MHz, CD_3OD, ppm) 6.10 (1H, m, H-6), 6.29 (1H, m, H-8), 6.79 (1H, m, H-2′), 7.65 (1H, m Hz, H-5′), 7.48 (1H, m, H-6′), 5.05 (1H, m, H-1′′), 3.25 (1H, m, H-2′′), 3.55 (1H, m, H-3′′), 3.71 (1H, m, H-4′′), 3.72/3.35 (2H, m, H-5′′); ^{13}C NMR (100 MHz, CD_3OD, ppm), 158.8 (C-2), 135.8 (C-3), 179.8 (C-4), 163.3 (C-5), 99.9 (C-6), 166.3 (C-7), 94.8 (C-8), 158.7 (C-9), 106.0 (C-10), 123.1 (C1′), 116.3 (C-2′), 146.1 (C-3′), 150.1(C-4′), 117.6 (C-5′), 123.1 (C-6′), 104.8 (C-1′′), 73.4 (C-2′′), 74.3 (C-3′′), 69.3 (C-4′′), 67.1 (C-5′′).

Quercetin (compound 5): Yellowish powder, UV λ_{max} 274 and 369 nm; ESI–MS m/z: $[M+H]^+$ 303.06, HRMS $[M+H]^+$ 303.0498, cald. for $C_{15}H_{11}O_7$ 303.0504 Da; ^{1}H NMR (400 MHz, CD_3OD, ppm) 6.01 (1H, d, *J* = 2.08 Hz, H-6), 6.21 (1H, d, *J* = 1.96 Hz, H-8), 7.56 (1H, d, *J* = 2.12 Hz, H-2′), 6.71 (1H, d, *J* = 8.48 Hz, H-5′), 7.47 (1H, dd, *J* = 7.44, 2.16 Hz, H-6′); ^{13}C NMR (100 MHz, CD_3OD, ppm), 148.9 (C-2), 137.4 (C-3), 177.4 (C-4), 162.6 (C-5), 99.4

(C-6), 165.7 (C-7), 94.5 (C-8), 158.3 (C-9), 104.6 (C-10), 124.3 (C1′), 116.1 (C-2′), 146.3 (C-3′), 148.1(C-4′), 116.4 (C-5′), 121.8 (C-6′).

3.6. LC–DAD–MS and LC–ESI–MS/MS Analyses

Liquid chromatography analyses were performed on a UPLC Acquity® (Waters, Milford, MA, USA) ion trap mass spectrometer according to the method developed by Fonseca et al. [60]. The analysis conditions were as follows: positive and negative ion mode; capillary voltage, 3500 V; capillary temperature, 320 °C; source voltage, 5 kV; vaporizer temperature, 320 °C; corona needle current, 5 mA; and sheath gas, nitrogen, and 27 psi. The analyses were run in full scan mode (100–2000 Da). The ESI–MS/MS analyses were additionally performed in a UPLC Acquity (Waters, Milford, MA, USA) with argon as the collision gas, and the collision energy was set at 30 eV. Chromatographic separation was performed on an Acquity UPLC BEH (1.7 µm, 50 × 2 mm i.d.) (Waters, Milford, MA, USA). The mobile phase consisted of water, 0.1% formic acid (solvent A), and acetonitrile 0.1% formic acid (solvent B). The elution protocol was 0–11 min, the linear gradient from 5% to 95% B. The flow rate was 0.3 mL min−1, and the sample injection volume was 4.0 µL. The UV spectra were registered from 190 to 450 nm. Mass spectrometry analysis was performed utilizing a Waters Acquity® TQD equipped (Waters, Milford, MA, USA) with a quadrupole instrument fitted in an electrospray source on a positive and negative ESI mode. Ion spray voltage: −4 kV; orifice voltage: −60 V.

3.7. High-Resolution Mass Spectrometry Analyses

High-resolution mass spectrometry analyses were performed according to the method described by Cruz et al. [21]. A Nexera UHPLC system (Shimadzu, Kyoto, Japan) combined with a maXis high-resolution ESI-QTOF mass spectrometer (Bruker) controlled by the Compass 1.7 software package (Bruker). A 5 µg sample was injected into a Shimadzu Shim-pack XR-ODS III column (C18, 2.2 µm, 2.0 × 150 mm) at 40 °C, with a flow rate of 400 µL/min. Mobile phases A and B (0.1% formic acid in Milli-Q water and acetonitrile, respectively) formed an eluent gradient from an initial 5 min of 5% B to 100% B in 40 min, with a hold at 100% B for 5 min. After UV–PDA detection (190–450 nm), mass spectra were acquired in positive mode at a rate of 5 Hz. Ion-source parameters were set to 500 V end-plate offset, 4500 V capillary voltage, 3.0 bar nebulizer pressure, and 8 L/min and 200 °C dry gas flow and temperature, respectively. Data-dependent fragment spectra were recorded using a collision energy range between 15 and 60 eV. Ion cooler settings were optimized for an m/z 100–1500 range, using a calibrant solution of 1 mM sodium formate in 50% 2-propanol. Mass calibration was achieved by initial ion-source infusion of 20 µL calibrant solution and postacquisition recalibration of the raw data. Compound detection was achieved by chromatographic peak dissection with subsequent formula determination according to the exact mass and isotope pattern (MS1). Putative identification was based on comparison of compound fragment spectra (MS2) with reference spectra from an in-house database of standard compounds (Fiocruz Minas), the public spectrum database MassBank, and in silico fragment spectra generated from the Universal Natural Product database [61,62].

3.8. Cytotoxicity Evaluation by MTT Assay

Cell suspensions (Vero and MRC-5) were distributed in 96-well microplates containing 6.0×10^4 cells/well. The plates were incubated in a humidified 5% CO_2 atmosphere at 37 °C for 24 h. Samples solubilized in dimethyl sulfoxide (DMSO) were diluted in culture medium supplemented with 1% SFB [48,49]. Substance dilutions ranged from 800 to 0.125 µg/mL. After the formation of the cell monolayer on the surface of the wells, the culture medium was removed, and 100 µL of diluted sample solutions along with 100 µL of 1% SFB-enriched culture medium were added, and the plates were incubated under the same atmospheric condition [63,64]. Seventy-two hours after the addition of samples, the culture medium was removed, and 28.0 µL of MTT solution (2.0 mg/mL in PBS) was added to

each well, and the plates were incubated again for 120 min. At the end of this period, 132 µL of DMSO was added to all wells, and the plates were shaken on a plate shaker for 15 min to dissolve the formed formazan [63,64]. Formazan quantification obtained by reducing tetrazolium salt in viable cells was performed on a Victor™ X3 microplate reader® (PerkinElmer, Waltham, MA, USA) using the WorkOut 2.5 software at 490 nm. Cell multiplication was compared with cell control. Cell toxicity was expressed in terms of 50% cytotoxic concentration (CC_{50}). The cytotoxic percentage was calculated as [(A-B)/A] × 100, where A and B are the optical densities at 490 nm (OD_{490}) from the wells where untreated (A) and treated (B) cells are present, respectively.

3.9. Evaluation of Anti–Zika Virus Activity

3.9.1. Preparation of Viral Suspensions

Zika virus (ZIKV) was picked on C6/36 cells to generate working stocks for 5 days at 28 °C. The infected cell culture supernatant was harvested after 5 days and clarified by centrifugation at 4000 RPM and refrigerated for 10 min at 4 °C, and then aliquoted and stored at −70 °C as virus stock until use.

3.9.2. Determination of Viral Infectious Titer by $TCID_{50}$

After the incubation period (24 h), for the formation of the Vero cell monolayer, the viral suspension was infected, containing in each well 100.0 µL of each dilution in 1% SFB DMEM medium. Viral stocks were diluted (10-1 to 10-18) and inoculated into Vero cell monolayers implanted in approximately 85% confluence 96-well plates (6×10^4 cells per well), maintaining three uninfected columns for cell control. The plates were then incubated at 37 °C (5% CO_2), and the cytopathic effect (ECP) was monitored. ECP was recorded every 24 h for 72 h, observing cell control.

3.9.3. Screening for Antiviral Activity by MTT Colorimetric Technique

It was performed according to the methodology described by Brandão et al. [30]. Sample stock solutions were prepared in DMSO (dimethyl sulfoxide) and evaluated at noncytotoxic concentrations. Vero cell monolayers were cultured in 96-well plates (6×10^4 cells per well). After 24 h of incubation in 5% CO_2 at 37 °C, the culture medium (DMEM 5% SFB) was removed, and 100.0 µL of sample dilutions were added to each well along with 100.0 µL of the viral suspension. Then, the cultures were incubated in a humid atmosphere containing 5% CO_2 at 37 °C for 72 h. Cell viability was assessed by the MTT colorimetric technique [37]. The supernatant was removed, and then 28.0 µL of an MTT solution (2.0 mg/mL in PBS) was added to each well. The plates were incubated for 2 h at 37 °C, and after this incubation time, 132.0 µL DMSO was added to each well to dissolve the formazan crystals. The plates were stirred for 15 min (Shaker New Brunswick Scientific C24), and the optical density was determined at 490 nm (OD_{490}) in a microplate reader.

The effective concentration that has 50% antiviral effect, or 50% effective concentration (EC_{50}), is expressed as the concentration that promotes the protection of 50% of treated cells from destruction caused by the virus. The percentage of protection was calculated as [(AB)/CB)] × 100, where A, B, and C are the OD_{490} of the wells, in which are present treated and infected (A), untreated and infected (B), and untreated and non-infected cells (C), respectively.

The selectivity index (SI), corresponding to the therapeutic index, is defined as the ratio of CC_{50} to EC_{50} values, and it shows the selectivity of the samples in inhibiting the virus multiplication cycle [37].

3.9.4. In Vitro Cytopathic Effect Inhibition Assay

In order to confirm the anti-ZIKV activity observed in the antiviral MTT assay, the Vero cell monolayer (9.5×10^6 cells per well) was infected by viral suspensions with titers of 1.0×10^7 $TCID_{50}$/mL, (MOI = 1), Zika virus, during 1 h for the viral adsorption. Afterwards, the viral suspension was removed and the wells were washed with PBS. Then,

the wells were treated with the active concentration of the compound (20 μg/mL) and ethanolic extract of leaves of *C. americana* (85 μg/mL). The plates were incubated at 37 °C in a humidified 5% CO_2 atmosphere and photographed 48 h after infection [17].

3.10. Statistical Analysis

Data from cytotoxicity and antiviral assays were evaluated according to their means and standard deviations. The cytotoxic concentration at 50% and the effective concentration at 50% were determined compared with the control obtained from nonlinear regression. These analyses were performed using the GraphPad Prism 5.04 statistical package® (GraphPad Software, Boston, MA, USA).

4. Conclusions

Curatella americana leaves are rich in phenolic compounds, mainly flavonoids. The bioguided phytochemical investigation of the ethanolic extract of *C. americana* leaves revealed that medium polarity constituents may be responsible for the observed anti-ZIKV activity, considering that only the ethyl acetate fraction obtained from the liquid–liquid partition of the ethanolic extract was active against ZIKV. From this fraction, three flavonoids were isolated: quercetin-3-*O*-hexosylgallate, quercetin-3-*O*-glucoside, and quercetin, in addition to a mixture (quercetin-3-*O*-rhamnoside and quercetin-3-*O*-arabinoside). Flavonoids can be considered primarily responsible for the antiviral activity observed, since the active substances obtained, quercetin-3-*O*-hexosylgallate and quercetin, showed significant biological activity, exhibiting selective and promising anti-ZIKV activity in vitro.

Supplementary Materials: The following supporting information can be downloaded at: https://www.mdpi.com/article/10.3390/molecules28062546/s1. Figure S1: ^{1}H NMR spectrum of Quercetin-3-*O*-hexosylgalate (**1**) (400 Hz, CD_3OD, δ); Figure S2: ^{13}C NMR spectrum of Quercetin-3-*O*-hexosylgalate (**1**) (100 Hz, CD_3OD, δ); Figure S3: DEPT-135° NMR spectrum of Quercetin-3-*O*-hexosylgalate (**1**) (100 Hz, CD_3OD, δ); Figure S4: COSY contour map of Quercetin-3-*O*-hexosylgalate (**1**) (400 Hz, CD_3OD, δ); Figure S5: HSQC contour map of Quercetin-3-*O*-hexosylgalate (**1**) (400 Hz, CD_3OD, δ); Figure S6: HMBC contour map of Quercetin-3-*O*-hexosylgalate (**1**) (400 Hz, CD_3OD, δ); Figure S7 ^{1}H NMR spectrum of Quercetin-3-*O*-glucoside (**2**) (400 Hz, CD^3OD, δ); Figure S8: ^{13}C NMR spectrum of Quercetin-3-*O*-glucoside (**2**) (100 Hz, CD_3OD, δ); Figure S9: DEPT-135° NMR spectrum of Quercetin-3-*O*-glucoside (**2**) (100 Hz, CD_3OD, δ); Figure S10: COSY contour map of Quercetin-3-*O*-glucoside (**2**) (400 Hz, CD_3OD, δ); Figure S11: HSQC contour map of Quercetin-3-*O*-glucoside (**2**) (400 Hz, CD_3OD, δ); Figure S12: HMBC contour map of Quercetin-3-*O*-glucoside (**2**) (400 Hz, CD_3OD, δ); Figure S13: ^{1}H NMR spectrum of Quercetin-3-*O*-rhamnoside (**3**) (400 Hz, CD_3OD, δ); Figure S14: ^{13}C NMR spectrum of Quercetin-3-*O*-rhamnoside (**3**) (100 Hz, CD_3OD, δ); Figure S15: DEPT-135° NMR spectrum of Quercetin-3-*O*-rhamnoside (**3**) (100 Hz, CD_3OD-d6, δ); Figure S16: COSY contour map of Quercetin-3-*O*-rhamnoside (**3**) (400 Hz, CD_3OD, δ); Figure S17: HSQC contour map of Quercetin-3-*O*-rhamnoside (**3**) (400 Hz, CD_3OD, δ); Figure S18: HMBC contour map of Quercetin-3-*O*-rhamnoside (**3**) (400 Hz, CD_3OD, δ); Figure S19: ^{1}H NMR spectrum of Quercetin-3-*O*-arabinoside (**4**) (400 Hz, CD_3OD, δ); Figure S20: ^{13}C NMR spectrum of Quercetin-3-*O*-arabinoside (**4**) (100 Hz, CD_3OD, δ); Figure S21: DEPT-135° NMR spectrum of Quercetin-3-O-arabinoside (**4**) (100 Hz, CD_3OD-d6, δ); Figure S22: COSY contour map of Quercetin-3-O-arabinoside (**4**) (400 Hz, CD_3OD-d6, δ); Figure S23: HSQC contour map of Quercetin-3-*O*-arabinoside (**4**) (400 Hz, CD_3OD, δ); Figure S24: HMBC contour map of Quercetin-3-*O*-arabinoside (**4**) (400 Hz, CD_3OD, δ); Figure S25: ^{1}H NMR spectrum of Quercetin (**5**) (400 Hz, CD_3OD, δ); Figure S26: ^{13}C NMR spectrum of Quercetin (**5**) (100 Hz, CD_3OD, δ); Figure S27: COSY contour map of Quercetin (**5**) (400 Hz, CD_3OD, δ); Figure S28: HSQC contour map of Quercetin (**5**) (400 Hz, CD_3OD, δ); Figure S29: HMBC contour map of Quercetin (**5**) (400 Hz, CD_3OD, δ).

Author Contributions: L.D.L., J.A.C.S. and G.M.V. conducted the entire phytochemical study. A.C.C.R., B.d.M.S., C.L.d.B.M. and L.F.d.M.T. contributed to the biological assays. M.K. contributed to the LC–MS analyses and orthographic corrections of the main text. G.C.B. contributed to the phytochemical study including the UPCL–DAD–MS analyses in the biological assays. All authors have read and agreed to the published version of the manuscript.

Funding: This work was supported by FAPEMIG (Fundação de Amparo à Pesquisa do Estado de Minas Gerais, Brazil), process number: CDS—APQ-00970-21, providing research resources for the acquisition of materials and equipment; PROPPI/UFOP public notice No. 03/2023; CNPq (Conselho Nacional de Desenvolvimento Científico e Tecnológico, Brazil)., providing fund for the APC fee; CAPES (Coordenação de Aperfeiçoamento de Pessoal de Ensino Superior, Brazil); and CNPq (Conselho Nacional de Desenvolvimento Científico e Tecnológico, Brazil), providing scholarships.

Institutional Review Board Statement: Not applicable.

Informed Consent Statement: Not applicable.

Data Availability Statement: Not applicable.

Acknowledgments: The authors would like to thank the La-boratório Multiusuário de Caracterização de Moléculas (LMCM) for providing NMR data. The authors are grateful for the support of the Federal University of Ouro Preto (UFOP) and the Coordination for the Improvement of Higher Education Personnel (CAPES).

Conflicts of Interest: The authors declare no conflict of interest.

Sample Availability: Not applicable.

References

1. Dick, G.W.A.; Kitchen, S.F.; Haddow, A.J. Zika virus (I). Isolations and serological specificity. *Transact. Royal. Soc. Trop. Med. Hyg.* **1952**, *46*, 509–520. [CrossRef] [PubMed]
2. Cerbino-Neto, J.; Mesquita, E.; Souza, T.; Parreira, V.; Wittlin, B.B.; Durovni, B.; Lemos, M.C.F.; Vizzoni, A.; De Filippis, A.M.B.; Sampaio, S.A.; et al. Clinical Manifestations of Zika Virus Infection, Rio de Janeiro, Brazil, 2015. *Emerg. Infect. Dis.* **2016**, *22*, 1318–1320. [CrossRef] [PubMed]
3. Solomon, T.; Baylis, M.; Brown, D. Zika virus and neurological disease—Approaches to the unknown. *Lancet Infect. Dis.* **2016**, *16*, 402–404. [CrossRef] [PubMed]
4. Govero, J.; Esakky, P.; Scheaffer, S.M.; Fernandez, E.; Drury, A.; Platt, D.J.; Gorman, M.J.; Richner, J.M.; Caine, E.A.; Salazar, V.; et al. Zika virus infection damages the testes in mice. *Nature* **2016**, *540*, 438–442. [CrossRef]
5. Yepez, J.B.; Murati, F.A.; Pettito, M.; Peñaranda, C.F.; de Yepez, J.; Maestre, G.; Arevalo, J.F.; Center, F.T.J.H.Z. Ophthalmic Manifestations of Congenital Zika Syndrome in Colombia and Venezuela. *JAMA Ophthalmol.* **2017**, *135*, 440–445. [CrossRef] [PubMed]
6. Calvet, G.; Aguiar, R.S.; Melo, A.S.O.; Sampaio, S.A.; de Filippis, I.; Fabri, A.; Araujo, E.S.M.; de Sequeira, P.C.; de Mendonça, M.C.L.; de Oliveira, L.; et al. Detection and sequencing of Zika virus from amniotic fluid of fetuses with microcephaly in Brazil: A case study. *Lancet Infect. Dis.* **2016**, *16*, 653–660. [CrossRef]
7. Thomas, D.L.; Sharp, T.M.; Torres, J.; Armstrong, P.A.; Munoz-Jordan, J.; Ryff, K.R.; Martinez-Quiñones, A.; Arias-Berríos, J.; Mayshack, M.; Garayalde, G.J.; et al. Local transmission of Zika virus—Puerto Rico, November 23, 2015–January 28, 2016. *Morb. Mort Weekly Rep.* **2016**, *65*, 154–158. [CrossRef]
8. Musso, D.; Baud, D.; Gubler, D. Zika virus: What do we know? *Clin. Microbiol. Infect.* **2016**, *22*, 494–496. [CrossRef]
9. Abbink, P.; LaRocca, R.A.; De La Barrera, R.A.; Bricault, C.A.; Moseley, E.T.; Boyd, M.; Kirilova, M.; Li, Z.; Ng'Ang'A, D.; Nanayakkara, O.; et al. Protective efficacy of multiple vaccine platforms against Zika virus challenge in rhesus monkeys. *Science* **2016**, *353*, 1129–1132. [CrossRef]
10. LaRocca, R.A.; Abbink, P.; Peron, J.P.S.; de A Zanotto, P.M.; Iampietro, M.J.; Badamchi-Zadeh, A.; Boyd, M.; Ng'Ang'A, D.; Kirilova, M.; Nityanandam, R.; et al. Vaccine protection against Zika virus from Brazil. *Nature* **2016**, *536*, 474–478. [CrossRef]
11. Pardi, N.; Weissman, D. Nucleoside Modified mRNA Vaccines for Infectious Diseases. *Methods Mol. Biol.* **2017**, *1499*, 109–121. [CrossRef] [PubMed]
12. Centers for Disease Control and Prevention. Available online: www.cdc.gov/zika/ (accessed on 22 February 2023).
13. Wong, S.S.-Y.; Poon, R.W.-S.; Wong, S.C.-Y. Zika virus infection—The next wave after dengue? *J. Formos. Med. Assoc.* **2016**, *115*, 226–242. [CrossRef] [PubMed]
14. Perry, H.; Khalil, A.; Aarons, E.; Russell, K.; O'Brien, P. Management of Zika virus in pregnancy: A review. *Br. Med. Bull.* **2017**, *124*, 157–169. [CrossRef] [PubMed]
15. Chattopadhyay, D.; Naik, T.N. Antivirals of Ethnomedicinal Origin: Structure-activity Relationship and Scope. *Mini Rev. Med. Chem.* **2007**, *7*, 275–301. [CrossRef] [PubMed]
16. De Clercq, E.; Field, H.J. Antiviral prodrugs-the development of successful prodrug strategies for antiviral chemotherapy. *Br. J. Pharmacol.* **2006**, *147*, 1–11. [CrossRef] [PubMed]
17. Reis, A.C.C.; Silva, B.M.; de Moura, H.M.M.; Pereira, G.R.; Brandão, G.C. Anti-Zika virus activity and chemical characterization by ultra-high performance liquid chromatography (UPLC-DAD-UV-MS) of ethanol extracts in Tecoma species. *BMC Complement. Med. Ther.* **2020**, *20*, 246. [CrossRef]

18. Reis, A.C.C.; de Moura, H.M.M.; Silva, B.M.; de Oliveira, A.B.; Brandão, G.C. Antiviral activity and chemical characterization of Cissus erosa (Vitaceae) ethanol extracts. *Rodriguésia* **2020**, *71*, 1–9. [CrossRef]
19. Ferreira, G.M.; Silva, B.D.M.; de Souza, G.H.B.; de Oliveira, A.B.; Brandão, G.C. Anti-Zika Activity of Ouratea semiserrata and Dereplication of Its Constituents. *Rev. Bras. Farm.* **2021**, *31*, 121–125. [CrossRef]
20. Reis, A.C.C.; Valente, G.M.; Silva, B.D.M.; Magalhães, C.L.D.B.; Kohlhoff, M.; Brandão, G.C. Anti-arboviral activity and chemical characterization of hispidulin and ethanolic extracts from *Millingtonia hortensis* L.f. and *Oroxylum indicum* (L.) Kurz (Bignoniaceae). *Nat. Prod. Res.* **2022**, *37*, 613–617. [CrossRef]
21. Dhole, A.E.; Yarasu, R.B.; Lata, D.B.; Baraskar, S.S.; Shaw, D. Mathematical modeling for the performance and emission parameters of dual-fuel diesel engine using producer gas as secondary fuel. *Biomass Convers. Bioref.* **2015**, *5*, 257–270. [CrossRef]
22. Doss, V.A.; Thangavel, K.P. Antioxidant and antimicrobial activity using different extracts of *Anacardium occidentale* L. *Int. J. Appl. Bio. Pharma Tech.* **2011**, *2*, 436–443.
23. Aquino, F.G.; Pereira, C.S.; Passos, F.B.; de Oliveira, M.C. Composição florística e estrutural de um cerrado sentido restrito na área de proteção de Manancial Mestre D'Armas, Distrito Federal. *Biosci. J.* **2014**, *30*, 564–575.
24. Alexandre-Moreira, M.S.; Piuvezam, M.R.; Araújo, C.C.; Thomas, G. Studies on the anti-inflammatory and analgesic activity of *Curatella americana* L. *J. Ethnopharmacol.* **1999**, *67*, 171–177. [CrossRef] [PubMed]
25. Felfili, J.M.; Nogueira, P.E.; Silva Júnior, M.C.D.; Marimon, B.S.; Delitti, W.B.C. Composição florística e fitossociologia do cerrado sentido restrito no município de Água Boa-MT. *Acta Bot. Bras.* **2002**, *16*, 103–112. [CrossRef]
26. Kissmann, K.G.; Groth, D. *Plantas infestantes e nocivas. Tomo 3: Plantas dicotiledôneas por orden de familias: Geraniaceae a Verbenaceae*; Basf: São Paulo, Brasil, 1995.
27. Guerrero, M.F.; Puebla, P.; Carrón, R.; Martın, M.L.; Arteaga, L.; San Román, L. Assessment of the antihypertensive and vasodi-lator effects of ethanolic extracts of some Colombian medicinal plants. *J. Ethnopharmacol.* **2002**, *80*, 37–42. [CrossRef]
28. Costa, E.S.; Hiruma-Lima, C.A.; Lima, E.O.; Sucupira, G.C.; Bertolin, A.O.; Lolis, S.F.; Andrade, F.D.P.; Vilegas, W.; Souza-Brito, A.R.M. Antimicrobial activity of some medicinal plants of the Cerrado, Brazil. *Phytot. Res. Int. J. Pharmacol. Toxicol. Eval. Nat. Prod. Derivat.* **2008**, *22*, 705–707. [CrossRef]
29. Hiruma-Lima, C.A.; Rodrigues, C.M.; Kushima, H.; Moraes, T.M.; de Fatima Lolis, S.; Feitosa, S.B.; Magri, L.P.; Soares, F.R.; Cola, M.M.; Andrade, F.D.P.; et al. The anti-ulcerogenic effects of *Curatella americana* L. *J. Ethnopharmacol.* **2009**, *121*, 425–432. [CrossRef]
30. De Toledo, C.E.M.; Britta, E.A.; Ceole, L.F.; Silva, E.R.; de Mello, J.C.; Dias Filho, B.P.; Nakamura, C.V.; Ueda-Nakamura, T. An-timicrobial and cytotoxic activities of medicinal plants of the Brazilian cerrado, using Brazilian cachaça as extractor liquid. *J. Ethnopharmacol.* **2011**, *133*, 420–425. [CrossRef]
31. De Toledo, C.E.M.; Santos, P.R.; de Mello, J.C.P.; Dias Filho, B.P.; Nakamura, C.V.; Ueda-Nakamura, T. Antifungal properties of crude extracts, fractions, and purified compounds from bark of *Curatella americana* L. (Dilleniaceae) against Candida species. *Evi.-Bas. Comp. Alt. Med.* **2015**, *2015*, 673962.
32. Lopes, R.H.O.; Macorini, L.F.B.; Antunes, K.Á.; Espindola, P.P.D.T.; Alfredo, T.M.; Rocha, P.D.S.D.; Pereira, Z.V.; dos Santos, E.L. Antioxidant and hypolipidemic activity of the hydroethanolic extract of *Curatella americana* L. leaves. *Oxi. Med. Cell. Long.* **2016**, *2016*, 9681425.
33. El-Azizi, M.M.; Ateya, A.M.; Svoboda, G.H.; Schiff, P.L., Jr.; Slatkin, D.J.; Knapp, J.E. Chemical constituents of Curatella americana (Dilleniaceae). *J. Pharml. Sci.* **1980**, *69*, 360–361. [CrossRef] [PubMed]
34. Fujishima, M.A.T.; Silva, N.D.S.R.D.; Ramos, R.D.S.; Ferreira, E.F.B.; dos Santos, K.L.B.; Silva, C.H.T.D.P.D.; da Silva, J.O.; Rosa, J.M.C.; dos Santos, C.B.R. An Antioxidant Potential, Quantum-Chemical and Molecular Docking Study of the Major Chemical Constituents Present in the Leaves of Curatella americana Linn. *Pharmaceuticals* **2018**, *11*, 72. [CrossRef] [PubMed]
35. Fujishima, M.A.T.; Sá, D.M.C.; Lima, C.M.D.S.; Bittencourt, J.A.H.M.; Pereira, W.L.A.; Muribeca, A.D.J.B.; e Silva, C.Y.Y.; da Silva, M.N.; de Sousa, F.F.O.; dos Santos, C.B.R.; et al. Chemical profiling of Curatella americana Linn leaves by UPLC-HRMS and its wound healing activity in mice. *PLoS ONE* **2020**, *15*, e0225514. [CrossRef] [PubMed]
36. Bézivin, C.; Tomasi, S.; Lohézic-Le Dévéhat, F.; Boustie, J. Cytotoxic activity of some lichen extracts on murine and human cancer cell lines. *Phytomedicine* **2003**, *10*, 499–503. [CrossRef] [PubMed]
37. Cos, P.; Vlietinck, A.J.; Berghe, D.V.; Maes, L. Anti-infective potential of natural products: How to develop a stronger in vitro 'proof-of-concept'. *J. Ethnopharmacol.* **2006**, *106*, 290–302. [CrossRef]
38. Yasumura, Y.; Kawakita, Y. Studies on SV40 in tissue culture-preliminary step for cancer research in vitro. *Nihon. Rinsho.* **1963**, *21*, 1201–1215.
39. Kim, W.Y.; Sharpless, N.E. The regulation of INK4/ARF in cancer and aging. *Cell* **2006**, *127*, 265–275. [CrossRef] [PubMed]
40. Osada, N.; Kohara, A.; Yamaji, T.; Hirayama, N.; Kasai, F.; Sekizuka, T.; Kuroda, M.; Hanada, K. The Genome Landscape of the African Green Monkey Kidney-Derived Vero Cell Line. *DNA Res.* **2014**, *21*, 673–683. [CrossRef]
41. Jacobs, J.P.; Jones, C.M.; Baille, J.P. Characteristics of a human diploid cell designated MRC-5. *Nature* **1970**, *227*, 168–170. [CrossRef]
42. MacKenzie, K.L.; Franco, S.; May, C.; Sadelain, M.; Moore, M.A. Mass cultured human fibroblasts overexpressing hTERT en-counter a growth crisis following an extended period of proliferation. *Exp. Cell Res.* **2000**, *259*, 336–350. [CrossRef]
43. Brandão, G.C.; Kroon, E.G.; Filho, J.D.S.; Oliveira, A.B. Antiviral Activity of *Fridericia formosa* (Bureau) L. G. Lohmann (Bignoniaceae) Extracts and Constituents. *J. Trop. Med.* **2017**, *2017*, 6106959. [CrossRef] [PubMed]
44. Dayem, A.A.; Choi, H.Y.; Kim, Y.B.; Cho, S.G. Antiviral effect of methylated flavonol isorhamnetin against Influenza. *PLoS ONE* **2015**, *10*, e0121610. [CrossRef] [PubMed]

45. Calland, N.; Sahuc, M.E.; Belouzard, S.; Pène, V.; Bonnafous, P.; Mesalam, A.A.; Deloison, G.; Descamps, V.; Sahpaz, S.; Wychowski, C.; et al. Polyphenols inhibit Hepatitis C virus entry by a new mechanism of action. *J. Virol.* **2015**, *89*, 10053–10063. [CrossRef] [PubMed]
46. Cotin, S.; Calliste, C.A.; Mazeron, M.C.; Hantz, S.; Duroux, J.L.; Rawlinson, W.D.; Ploy, M.; Alain, S. Eight flavonoids and their potential as inhibitors of human Cytomegalovirus replication. *Antiviral. Res.* **2012**, *96*, 181–186. [CrossRef] [PubMed]
47. Frabasile, S.; Koishi, A.C.; Kuczera, D.; Silveira, G.F.; Verri, W.A.; Duarte dos Santos, C.N.; Bordignon, J. The citrus flavanone naringenin impairs Dengue virus replication in human cells. *Sci. Rep.* **2017**, *7*, 41864. [CrossRef] [PubMed]
48. Wong, G.; He, S.; Siragam, V.; Bi, Y.; Mbikay, M.; Chretien, M.; Qiu, X. Antiviral activity of quercetin-3-β-OD-glucoside against Zika virus infection. *Virol. Sin.* **2017**, *32*, 545–547. [CrossRef] [PubMed]
49. Mounce, B.C.; Cesaro, T.; Carrau, L.; Vallet, T.; Vignuzzi, M. Curcumin inhibits Zika and Chikungunya virus infection by inhibiting cell binding. *Antiv. Res.* **2017**, *142*, 148–157. [CrossRef] [PubMed]
50. Gaudry, A.; Bos, S.; Viranaicken, W.; Roche, M.; Krejbich-Trotot, P.; Gadea, G.; Desprès, P.; El-Kalamouni, C. The flavonoid isoquercitrin precludes initiation of Zika virus infection in human cells. *Int. J. Mol. Sci.* **2018**, *19*, 1093. [CrossRef]
51. Sharma, N.; Murali, A.; Singh, S.K.; Giri, R. Epigallocatechin gallate, an active green tea compound inhibits the Zika virus entry into host cells via binding the envelope protein. *Int. J. Bio. Macromol.* **2017**, *104*, 1046–1054. [CrossRef]
52. Di Petrillo, A.; Orrù, G.; Fais, A.; Fantini, M.C. Quercetin and its derivates as antiviral potentials: A comprehensive review. *Phytother. Res.* **2021**, *36*, 266–278. [CrossRef]
53. Roy, A.; Lim, L.; Srivastava, S.; Lu, Y.; Song, J. Solution conformations of Zika NS2B-NS3pro and its inhibition by natural products from edible plants. *PLoS ONE* **2017**, *12*, e0180632. [CrossRef] [PubMed]
54. Lim, H.J.; Nguyen, T.T.H.; Kim, N.M.; Park, J.S.; Jang, T.S.; Kim, D. Inhibitory effect of flavonoids against NS2B-NS3 protease of Zika virus and their structure activity relationship. *Biotechnol. Lett.* **2017**, *39*, 415–421. [CrossRef] [PubMed]
55. Zou, M.; Liu, H.; Li, J.; Yao, X.; Chen, Y.; Ke, C.; Liu, S. Structure-activity relationship of flavonoid bifunctional inhibitors against Zika virus infection. *Biochem. Pharmacol.* **2020**, *177*, 113962. [CrossRef] [PubMed]
56. Kadota, S.; Takamori, Y.; Nyein, K.N.; Kikuchi, T.; Tanaka, K.; Ekimoto, H. Constituents of the leaves of Woodfordia fruticosa Kurz. I: Isolation, structure, and proton and carbon-13 nuclear magnetic resonance signal assignments of Woodfruticosin (Woodfordin C), an inhibitor of deoxyribonucleic acid topoisomerase II. *Chem. Pharm. Bull.* **1990**, *38*, 2687–2697. [CrossRef] [PubMed]
57. Lee, M.H.; Son, Y.K.; Han, Y.N. Tissue factor inhibitory flavonoids from the fruits of Chaenomeles sinensis. *Arch. Phar. Res.* **2002**, *25*, 842–850. [CrossRef] [PubMed]
58. Ren, G.; Hou, J.; Fang, Q.; Sun, H.; Liu, X.; Zhang, L.; Wang, P.G. Synthesis of flavonol 3-O-glycoside by UGT78D1. *Glycoconj. J.* **2012**, *29*, 425–432. [CrossRef]
59. Li, Y.-L.; Li, J.; Wang, N.-L.; Yao, X.-S. Flavonoids and a New Polyacetylene from Bidens parviflora Willd. *Molecules* **2008**, *13*, 1931–1941. [CrossRef]
60. Da Fonseca, J.M.; Reis, A.C.C.; Pereira, G.R.; de Moura, H.M.M.; Filho, J.D.S.; Silva, B.D.M.; Brandão, G.C. Chromatographic profile of xanthones and flavonoids in the anti-dengue extracts of Fridericia samydoides (Cham.) L.G. Lohmann (Bignoniaceae). *Braz. J. Pharm. Sci.* **2022**, *58*, 1–15. [CrossRef]
61. Horai, H.; Arita, M.; Kanaya, S.; Nihei, Y.; Ikeda, T.; Suwa, K.; Ojima, Y.; Kenichi, T.; Satoshi, T.; Ken, A.; et al. MassBank: A public repository for sharing mass spectral data for life sciences. *J. Mass. Spectrom.* **2010**, *45*, 703–714. [CrossRef]
62. Allard, P.M.; Péresse, T.; Bisson, J.; Gindro, K.; Marcourt, L.; Pham, V.C.; Roussi, F.; Litaudon, M.; Wolfender, J.L. Integration of Molecular Networking and In-Silico MS/MS Fragmentation for Natural Products Dereplication. *Anal. Chem.* **2016**, *88*, 3317–3323. [CrossRef]
63. Mosmann, T. Rapid colorimetric assay for cellular growth and survival: Application to proliferation and cytotoxicity assays. *J. Immun. Met.* **1983**, *65*, 55–63. [CrossRef] [PubMed]
64. Twentyman, P.R.; Luscombe, M. A study of some variables in a tetrazolium dye (MTT) based assay for cell growth and chemo-sensitivity. *Br. J. Cancer* **1987**, *56*, 279. [CrossRef] [PubMed]